Proceedings of the 7th International Symposium on Cavitation
CAV2009 – Paper No. 70
August 17-22, 2009, Ann Arbor, Michigan, USA

Rudder Gap Flow Control for Cavitation Suppression

Jungkeun Oh
Inha Univ.
Incheon, Korea

Hee Bum Lee
Seoul National Univ.
Seoul, Korea

Kwangho Shin
Seoul National Univ.
Seoul, Korea

Changmin Lee
Seoul National Univ.
Seoul, Korea

Shin Hyung Rhee
Seoul National Univ.
Seoul, Korea

Jung Chun Suh
Seoul National Univ.
Seoul, Korea

Hyochul Kim
Inha Univ.
Incheon, Korea

ABSTRACT

For the suppression of rudder cavitation, especially within and around the gap between the stationary and movable parts, flow control devices were developed. In the present study, both experimental and computational analyses of the flow control devices were carried out. The new rudder system is equipped with cam devices, which effectively close the gap between the stationary horn/pintle and movable flaps. Model scale experiments of surface pressure measurements, flow field visualization near the gap using PIV, and cavitation behavior observation were conducted in a cavitation tunnel. The experiments were simulated using a computational fluid dynamics tool and the results are compared for validation. It is confirmed that the flow control devices effectively suppresses the rudder gap cavitation and, at the same time, augments lift.

INTRODUCTION

Nowadays, the cavitation of the rudder system is frequently observed because cargo ships, such as container ships, are larger and faster. When a ship is in straight cruising state, the cavitation of the rudder system causes more serious erosion due to the long cruising time than in maneuvering state. The erosion on the rudder system is detrimental to the ship safety and cost-effectiveness. The cavitation in the horn-type rudder system takes place around the leading edge and gap region of the rudder system. The former cavitation can be mitigated by altering rudder section [1-3] and the latter by reducing gap clearance between the stationary horn/pintle part and movable flaps of rudder system. The gap clearance, however, cannot be controlled easily because the stationary horn/pintle part, which is usually cast, has a production error and the safety margin of assemblage to avoid the interference between the stationary part and movable part. The gap clearance in the rudder system is normally known as about *50mm*. Figure 1 shows erosion on rudder system which is marked with yellow dotted line; the cavitation around gap region seems more severe than around leading edge.

Figure 1: Erosion on rudder by the cavitation (marked with yellow dotted line)

There have been several interesting studies on the suppression of this rudder cavitation with modified rudder shapes and/of various types of devices attached to the region inside or around the gap [4-7]. However, many of them lack completeness in terms of suppressing the rudder cavitation and do not consider the devices to increase the rudder performance.

In the present study, a newly devised rudder system, which is recently proposed by the authors, is analyzed with regard to the cavitation suppression and lift augmentation. The new rudder system differs from conventional ones in the cam devices, which effectively close the gap between the stationary horn/pintle and movable flaps. Results from both model tests

and numerical simulations using a computational fluid dynamics (CFD) code are presented.

Model tests were carried out in a cavitation tunnel at Seoul National University, Korea. First, the surface pressure distribution on the two-dimensional (2D) rudder section was measured, so the effects of the blocking devices on cavitation suppression and lift augmentation are accounted. Second, the velocity field near the gap was visualized and analyzed using the particle image velocimetry (PIV) techniques. Third, the cavitation behavior was observed. By depressurizing the flow in the tunnel, it is possible to identify the incipient cavitation number at which the cavitation starts to take place and the developing behavior of the cavitation.

For the present study two CFD codes, namely and FLUENT, were selected. The CFD codes solve the Reynolds-averaged Navier-Stokes equations for the same problems done in the experiments. The computational results were compared with the experimental data in terms of the surface pressure distribution, velocity field near the gap, and cavitation inception with the open- and closed gap.

GAP FLOW CONTROL DEVICES AND TEST MODEL

The main difference of the new rudder system from the conventional ones is found near the gap between the stationary horn/pintle and movable flaps [8]. Figure 3 shows the conventional and new rudder system at deflection angle of 5^o; the yellow bars are gap flow control devices. Gap flow control devices in horn and pintle sections has different size and direction because of the different location and local shape, but the main principle operated with cam is the same, shown in Figure 2. Gap flow devices are designed to block the gap flow about 95% when the deflection angle is 3^o and more. By blocking the flow through the gap, (1) the pressure difference on the sides of stationary part increases, which results in the lift augmentation, and (2) the negative pressure peaks are removed or mitigated, which eventually results in cavitation suppression.

In the present study, NACA0020 section was selected, which is similar to the typical rudder section and has adequate thickness for assembling individual part of the models and for placing the pressure measuring holes. Two models were designed and manufactured with aluminum alloy for two-dimensional experiments: one is horn section and the other is pintle section. The outlines of each section are shown in Figure 4. The chord and span length of each model are *200mm* and *150mm*, respectively.

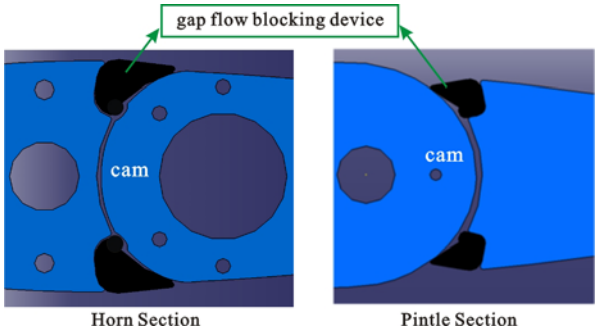

Figure 2: gap flow blocking device in horn and pintle section

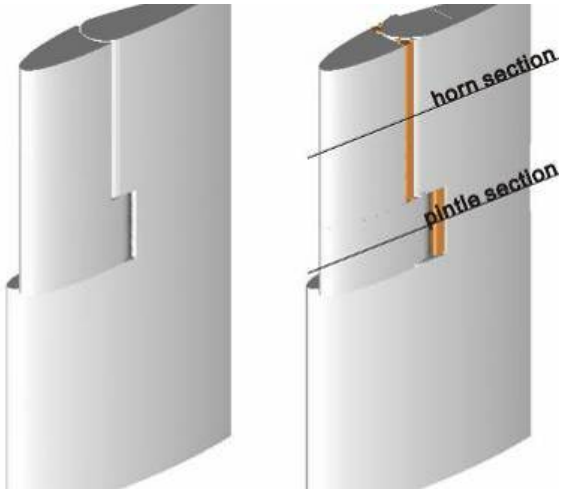

Figure 3: three dimensional views of rudder systems

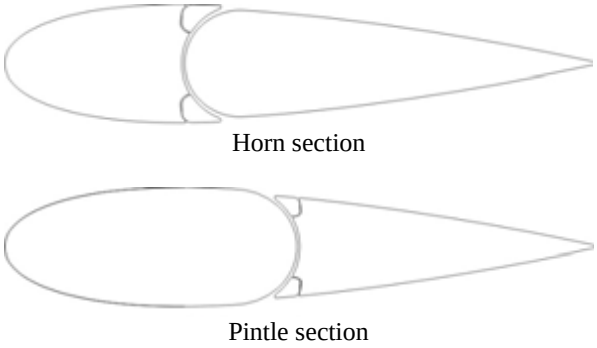

Figure 4: 2D model shape

EXPERIMENTAL FACILITY

Surface pressure measurements, velocity measurements with PIV technique and cavitation visualization were carried out in the cavitation tunnel at Seoul National University (Figure 5). The measurement section of this facility is $1m^L$ x $0.15m^W$ x $0.5m^H$. The controllable pressure range is *15kPa* to *300kPa* and the maximum flow speed is *16m/s*.

Figure 5: Cavitation tunnel at Seoul National University

SURFACE PRESSURE MEASUREMENTS

Two models, one for the horn section and the other for the pintle section, were manufactured to accommodate the holes and tubing inside the model. Figure 6 shows the models manufactured for the surface pressure measurement. Each model was fixed to a circular end plate and the angle of attack is adjusted by simply rotating the end plate. Figure 7 shows the locations of pressure measuring holes of each section. There were 37 holes on the horn section model and 39 holes on the pintle section model. The holes were determined carefully in such a way that there exists no interference between holes, i.e., around mid-span with a *3mm* interval, along a line that makes approximately a five degree inclination angle with the flow direction. The diameter of each hole is *2mm*. Figure 8 shows a schematic diagram of the experiments in the cavitation tunnel with a pressure transducer attached to a scanivalve. The flow speed was set to *7m/s* and Reynolds number based on chord length was $1.4x10^6$. Surface pressure measurements were carried out at deflection angle of 0°, 3°, and 5° when the gap was open and closed. These test conditions are listed in Table 1.

In order to compare open gap and closed gap, surface pressure is represented with negative pressure coefficient ($-C_p$). The negative pressure coefficient ($-C_p$) is defined as:

$$-C_p = \frac{P_A - P_{foil}}{\frac{1}{2}\rho V_A^2} \qquad (1)$$

where P_A is the reference pressure at the point A in Figure 8, P_{foil} the surface pressure of each pressure hole of the model, V_A the inflow velocity, and ρ the water density.

The results are displayed in Figure 9 and Figure 10; Figure 9 is for the horn section and Figure 10 for the pintle section. The empty and filled symbol in each figure represent open and closed gap, respectively. These results show that (1) when the gap was closed, the pressure peaks were diminished near the gap region, especially in horn section (Figure 9) (2) the pressure differences between pressure side and suction side on each section were increased. Therefore, it is confirmed that the cavitation near the gap is suppressed by the gap flow control devices and the rudder force is increased due to blocking gap flow.

Horn section model Pintle section model

Figure 6: Models for surface pressure measurement

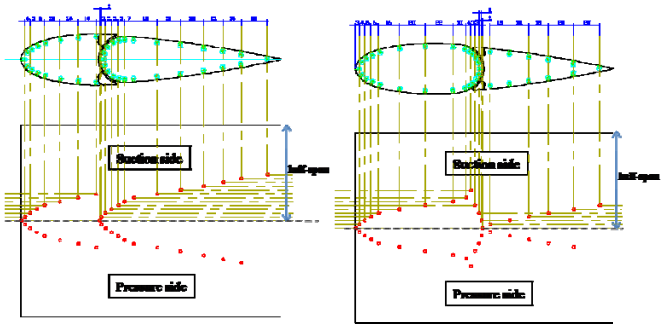

Horn section model Pintle section model

Figure 7: Pressure measuring holes of each model

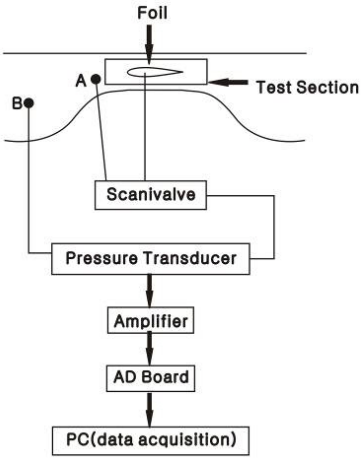

Figure 8: Schematic diagram of surface pressure measurement

Table 1: Test conditions of surface pressure measurements

Reynolds number (Velocity)	Model	Gap status	deflection Angle
$1.4x10^6$ (7m/s)	Horn Section	Open gap	0
			3
			5
		Closed gap	0
			3
			5
	Pintle Section	Open gap	0
			3
			5
		Closed gap	0
			3
			5

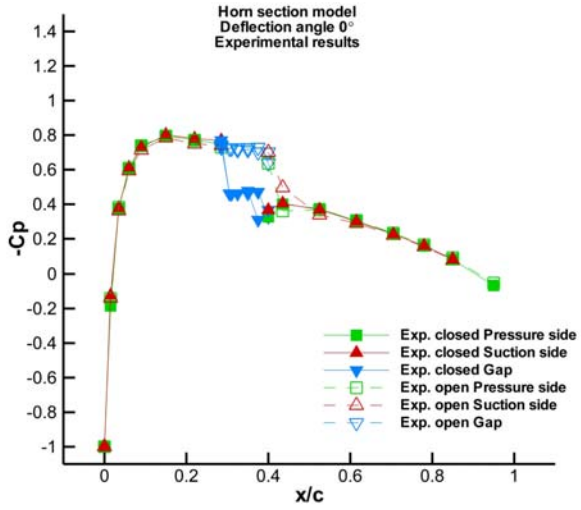

0 degree

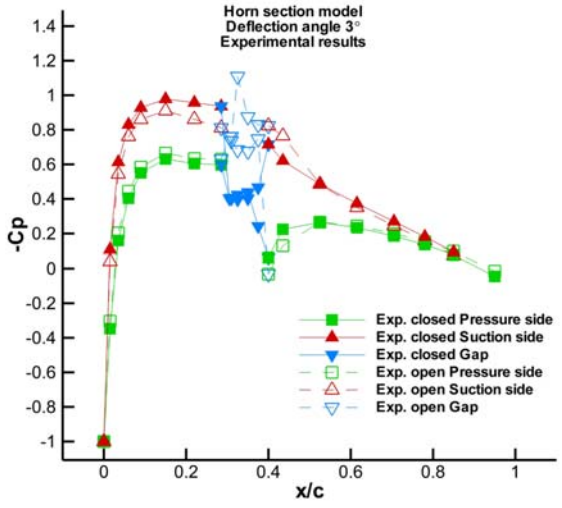

3 degrees

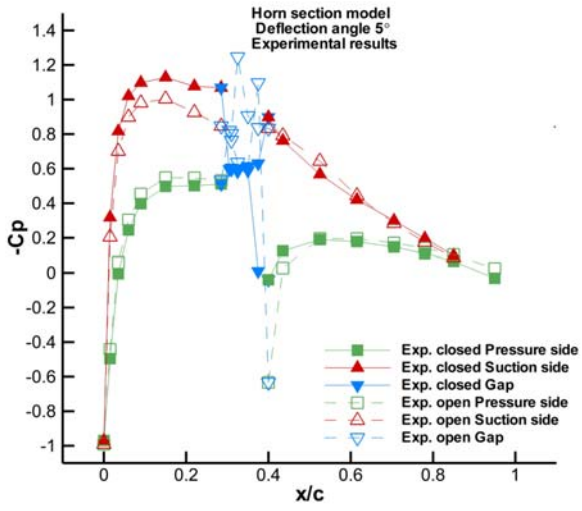

5 degrees

Figure 9: Experimental results for **s**urface pressure measurement of horn section
(empty symbol: open gap, filled symbol: closed gap)

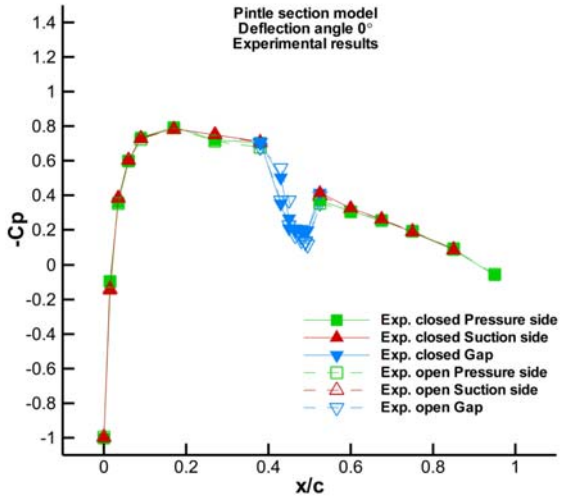

0 degree

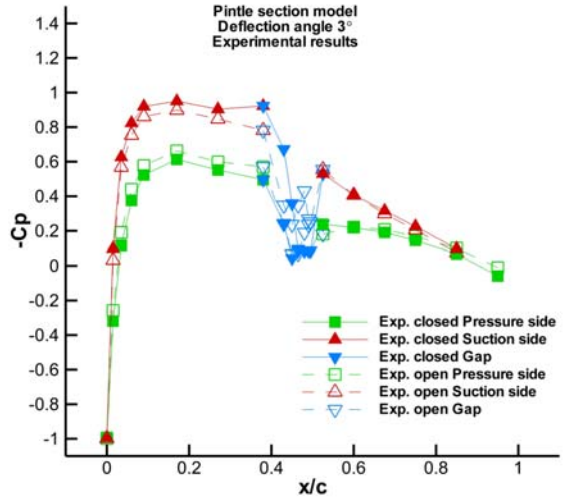

3 degrees

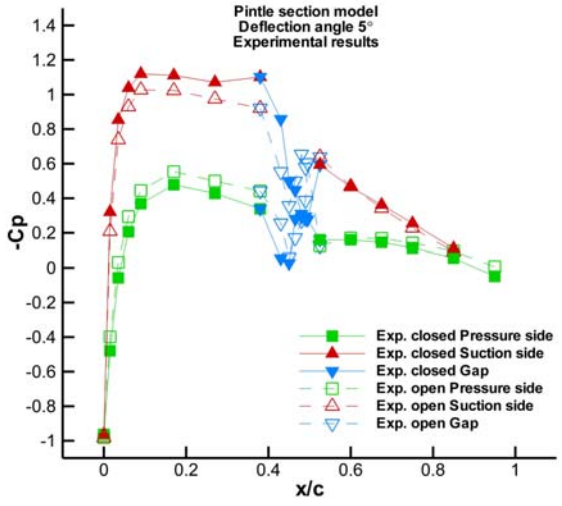

5 degrees

Figure 10: Experimental results for **s**urface pressure measurement of pintle section
(empty symbol: open gap, filled symbol: closed gap)

In order to validate these experimental results and make up for the unmeasurable location due to the gap flow control devices for each model, numerical simulations were conducted using the computational fluid dynamics (CFD) code, FLUENT.

The computational results were obtained by solving the Reynolds-averaged Navier-Stokes (RANS) equations.

$$\frac{\partial \rho}{\partial t} + \nabla \cdot (\rho \vec{v}) = 0 \qquad (2)$$

$$\frac{\partial}{\partial t}(\rho \vec{v}) + \nabla \cdot (\rho \vec{v} \vec{v}) = -\nabla p + \nabla \cdot (\bar{\bar{\tau}}) \qquad (3)$$

where $\vec{v}$ is the velocity vector in the Cartesian coordinate system, p the static pressure, and $\bar{\bar{\tau}}$ the stress tensor.

The CFD code, FLUENT 6.2, employs a cell-centered finite-volume method. Convective terms are discretized using the second order accurate upwind scheme, while diffusive terms are discretized using the second order accurate central differencing scheme. The velocity-pressure coupling and overall solution procedure are based on a SIMPLEC type segregated algorithm. The convergence criteria in the present study were at least three orders of magnitude drop in the mass conservation imbalance and momentum equation residuals, which are deemed sufficient for most steady flow solutions.

Once the Reynolds averaging approach for turbulence modeling is applied, the Reynolds stresses resulting from the process must be modeled to close Equation (2). The so-called realizable k-ε turbulence model [9], which is based on the Boussinesq hypothesis with transport equations for the turbulent kinetic energy, k, and its dissipation rate, ε, was used for turbulence closure. The turbulent viscosity μ_t was computed by combining k and ε as $\mu_t = \rho C_\mu k^2/\varepsilon$, where C_μ is a function of the mean strain and rotation rates, the angular velocity of the system rotation, and k and ε. The realizable k-ε model is a variation of the standard k-ε model and has shown good performance for flows with strong streamline curvature, vortices, and rotation [8,10,11]. For wall boundary conditions, the wall function approach based on the law of the wall was applied.

For corresponding computations, the domain extent was set to match the test section dimensions of the cavitation tunnel, except in the flow direction to ensure the proper inflow and outflow boundary conditions. Figure 11 and Figure 12 show the computational domain and grids, respectively. Fully structured grids were generated with approximately 54,000 cells total, and the first cell height was set to 110 in terms of y+. The computational conditions are the same as those for the experiments.

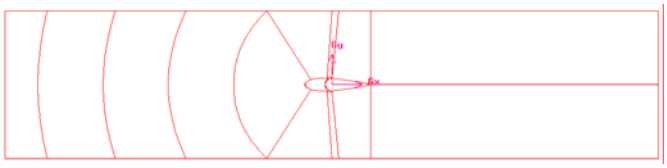

Figure 11: 2D computational domain

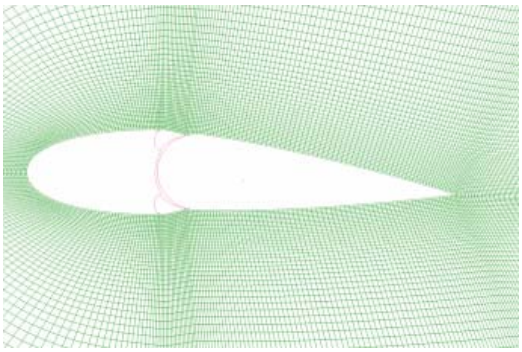

Horn section

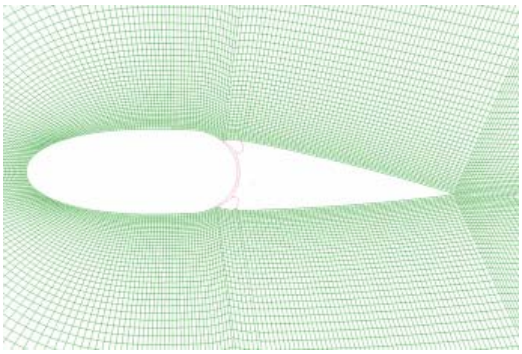

Pintle section

Figure 12: 2D computational domains around the models

Comparison results between experiments and computations are shown in Figure 13 ~ Figure 16. Figure 13 and Figure 14 are comparison results for the horn section with open and closed gap, respectively, and Figure 15 and Figure 16 for the pintle section. These figures show that experiments and computations are matched well and the pressure peaks in the vicinity of gap are presented in computational results, which couldn't measure in experiments.

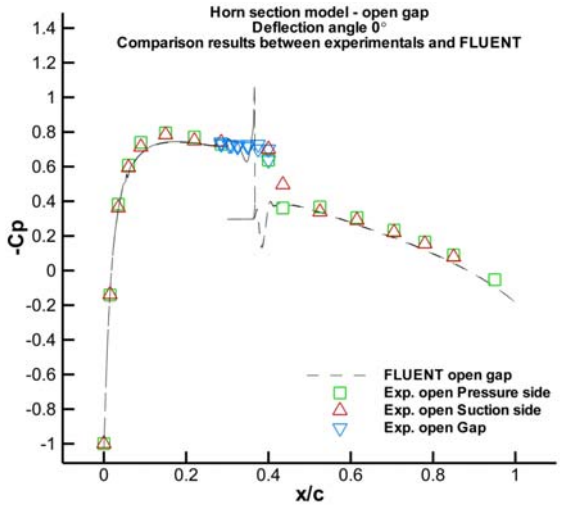

0 degree

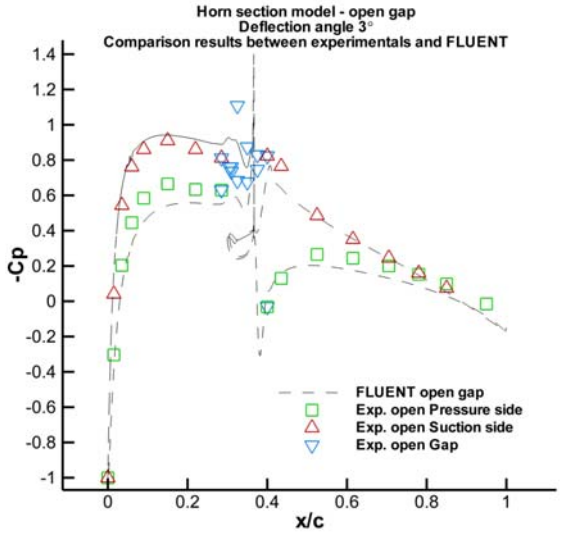

3 degrees

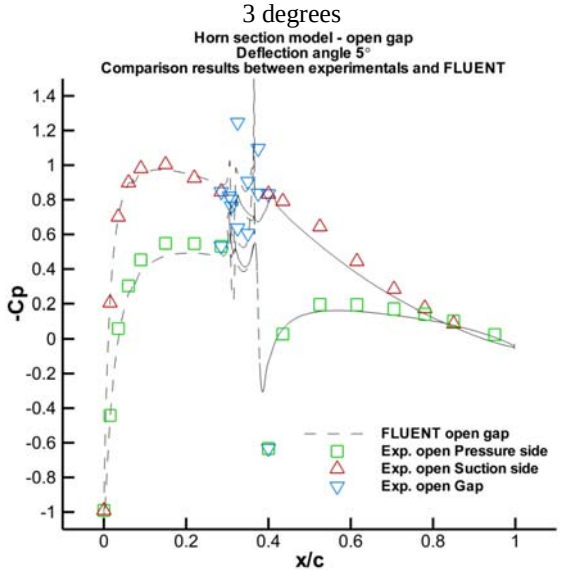

5 degrees

Figure 13: Comparison results of the horn section between experiments (empty symbol) and computations (dashed line) with open gap

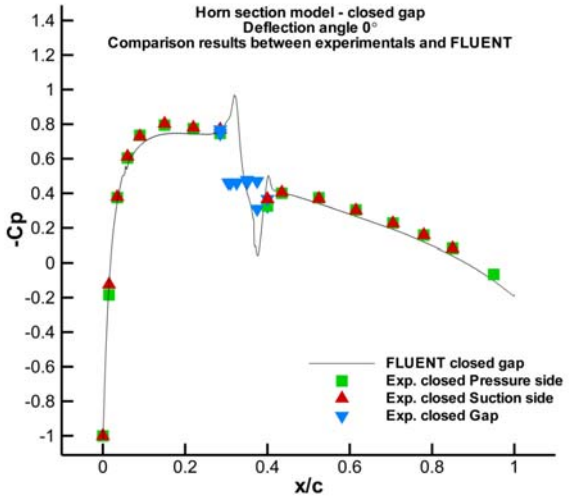

0 degree

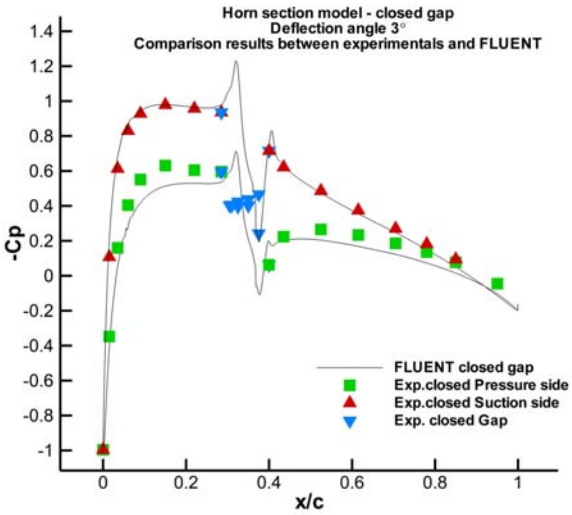

3 degrees

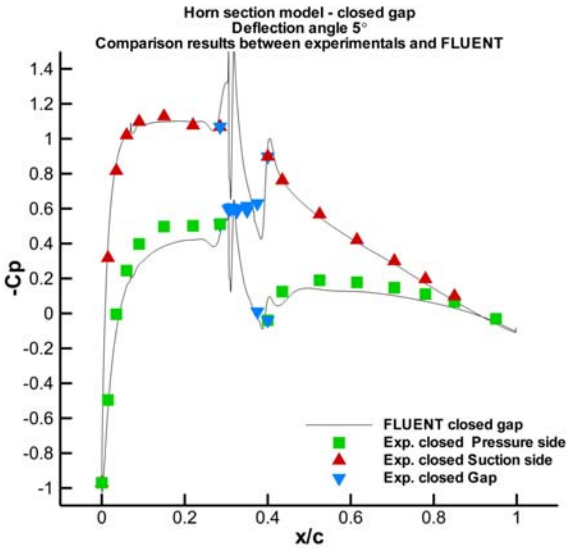

5 degrees

Figure 14: Comparison results of the horn section between experiments (empty symbol) and computations (dashed line) with closed gap

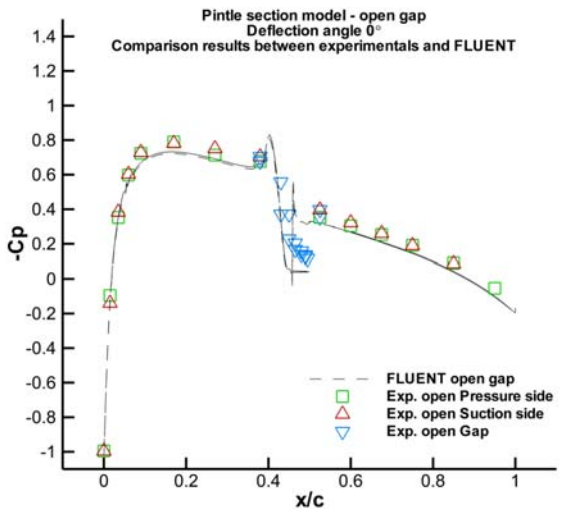

0 degree

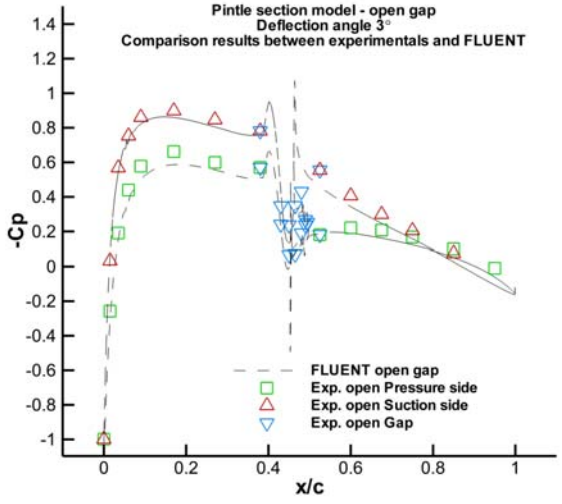

3 degrees

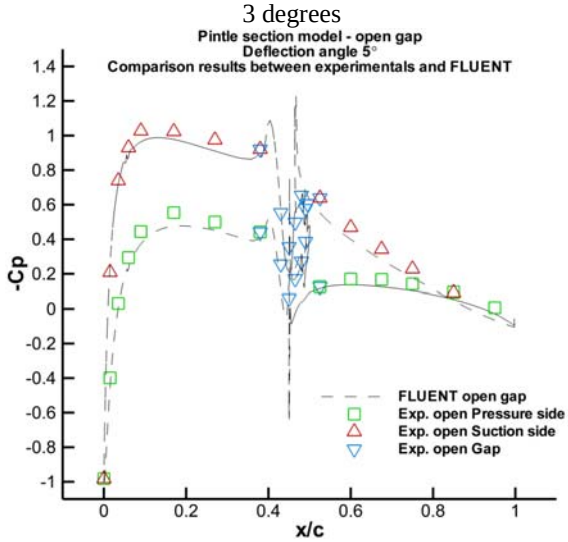

5 degrees

Figure 15: Comparison results of the pintle section between experiments (empty symbol) and computations (dashed line) with open gap

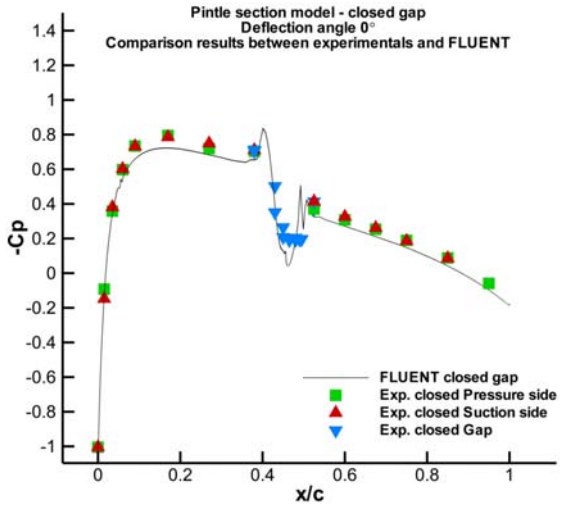

0 degree

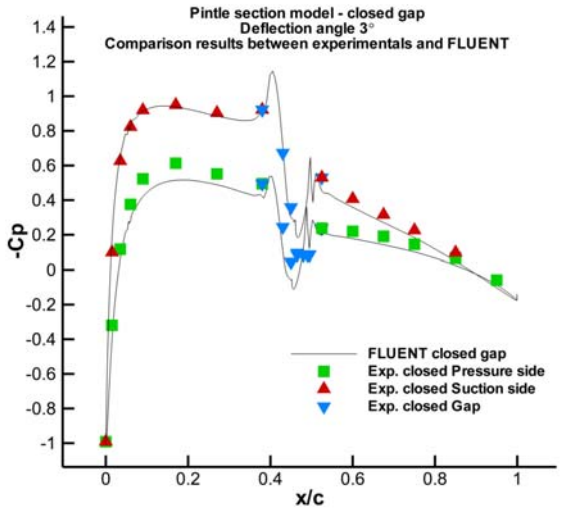

3 degrees

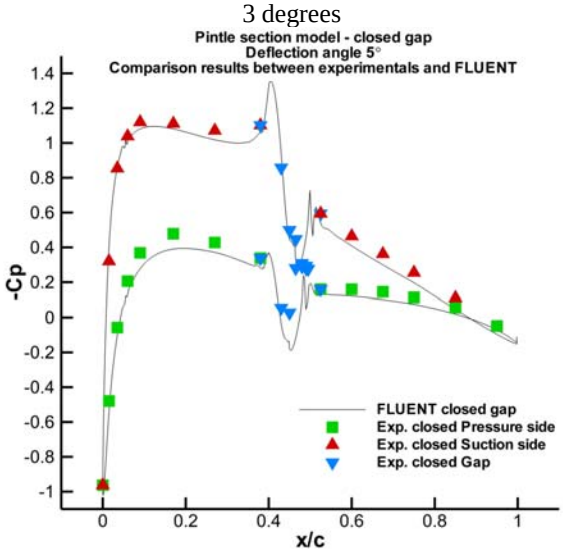

5 degrees

Figure 16: Comparison results of the pintle section between experiments (empty symbol) and computations (dashed line) with closed gap

VELOCITY FIELD VISUALIZATION NEAR THE GAP

In order to prevent the reflection of the laser, another set of models was manufactured for the velocity field and cavitation behavior visualization. PIV system for these test are 200mJ two head pulse-type laser, 2k x 2k CCD camera, and synchronizer. Figure 17 shows the experimental setup for these tests and Figure 18 the field of view. In these tests, horn section model was only used and the deflection angle was 5^o, but the pressure side and suction side were measured. For the same measuring ranges of each test condition, PIV systems were fixed like Figure 17, illuminated under the test section of cavitation tunnel, and the movable flaps' angle was changed; counterclockwise 5^o for suction side and clockwise 5^o for pressure side.

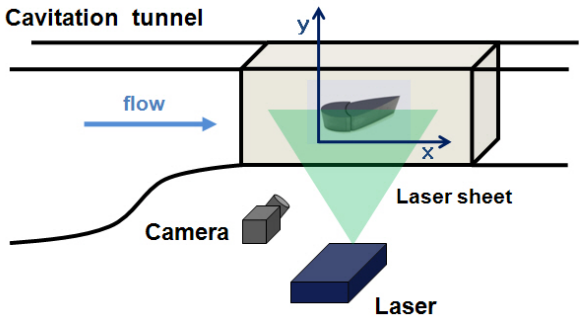

Figure 17: Experimental setup for PIV in the cavitation tunnel

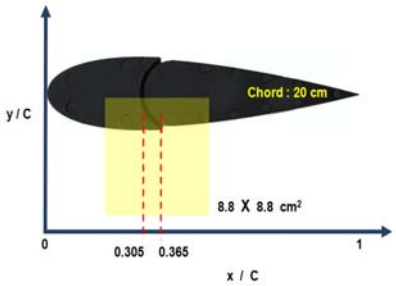

Figure 18: Areas of interest for velocity field visualization

Figure 19~ Figure 21 show velocity magnitude, x-directional velocity, y-directional velocity of the suction side, and Figure 22 ~ Figure 24 show those of the pressure side. From these results, it is found that when gap is closed, the velocity field of the suction side was increased and one of the pressure side was decreased on the whole, but in the vicinity of the gap in the pressure side, especially, the velocity field were locally increased due to the gap flow.

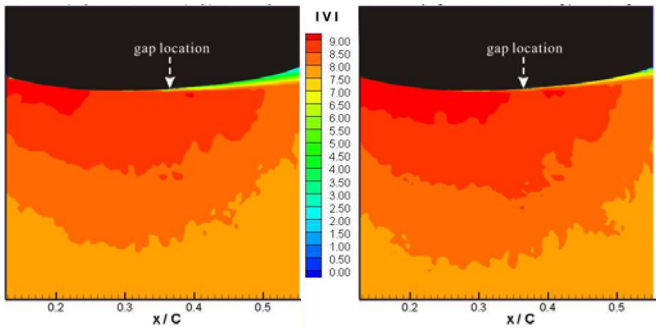

Open gap Closed gap

Figure 19: Velocity magnitude contours of the suction side at 5 degrees

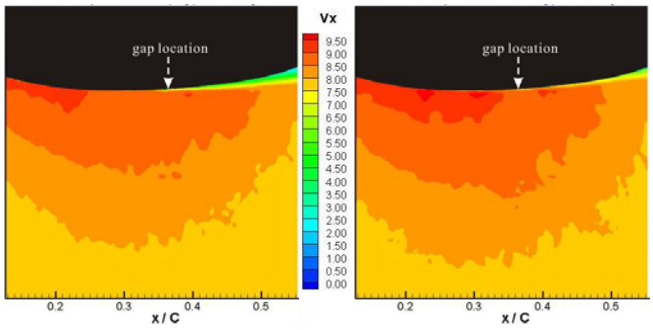

Open gap Closed gap

Figure 20: x-directional velocity contours of the suction side at 5 degrees

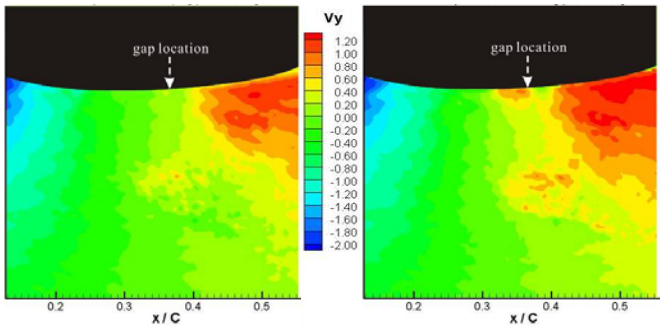

Open gap Closed gap

Figure 21: y-directional velocity contours of the suction side at 5 degrees

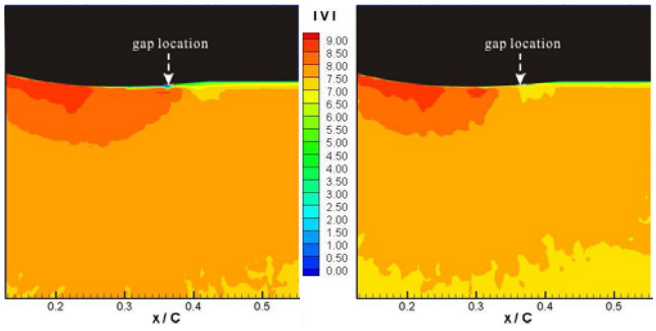

Open gap Closed gap

Figure 22: Velocity magnitude contours of the pressure side at 5 degrees

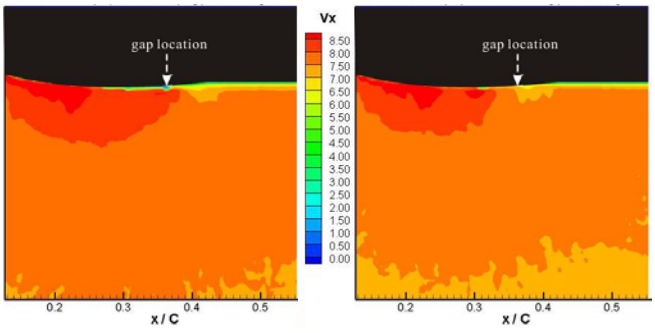

Open gap Closed gap

Figure 23: x-directional velocity contours of the pressure side at 5 degrees

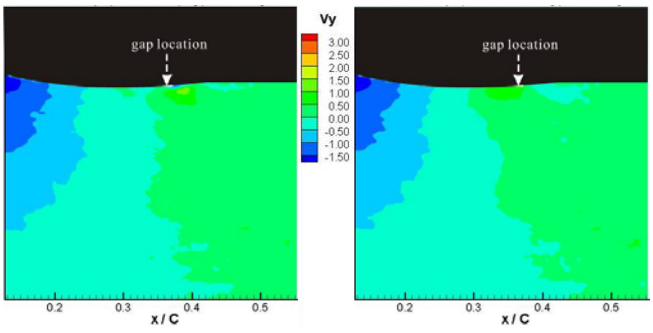

Open gap Closed gap

Figure 24: y-directional velocity contours of the pressure side at 5 degrees

CAVITATION VISUALIZATION

The cavitation visualizations were carried out with the same test conditions as those for the pressure measurements; deflection angles of 0^o, 3^o, and 5^o of each model with open/closed gap, constant inflow speed of 7 m/s. In order to identify the incipient cavitation number, increasing depressurization is applied to make the cavitation number based on the inflow speed and tunnel reference pressure decreases.

The cavitation number is defined as:

$$\sigma = \frac{P_A - P_v}{\frac{1}{2}\rho V_A^2} \qquad (4)$$

where P_A is the reference pressure at the point A in Figure 8, P_v the vapor pressure, V_A the inflow velocity, and ρ the water density.

In order to make it easy to observe the incipient cavitation, the suction side was placed downward.

In these experiments, the cavitation inception was checked in the following way. First, the model was set in the tunnel with deflection angles of 0^o, 3^o, and 5^o. When applying the deflection angle, the movable flap was rotated in the counter-clockwise direction so that the visualization could be done through the bottom window of the test section. The flow speed was set to *7m/s*. while gradually depressurizing the tunnel, careful observation was made on the foil surface using a video monitor. Once the cavity was observed, put a hold on the depressurization and recorded the cavitation behavior using a video camera.

Figure 25 and Figure 26 show the cavity on the rudder surface at the incipient cavitation number with the open- and closed gap for the horn and pintle section, respectively. From these results, it is found that when the gap was closed, the incipient cavitation number (σ) was lower than when the gap was closed except the horn section at deflection angle of 0^o. Moreover, while the location of the incipient cavitation with open gap was in the vicinity of gap, one with closed gap was not near the gap but the location moved toward the leading edge. The incipient cavitation number and locations of each test condition are listed in Table 2 and Table 3.

Table 2 Comparison cavitation locations and incipient numbers of the horn section between open and closed gap (c : chord)

Deflection angle	Open gap cavitation inception No. (location)	Closed gap cavitation inception No. (location)
0	1.66 (0.38c)	1.17 (0.325c)
3	1.48 (0.38c)	1.40 (0.325c)
5	1.70 (0.35c)	1.43 (0.3c)

σ=1.66 at 0.38c σ=1.17 at 0.325c

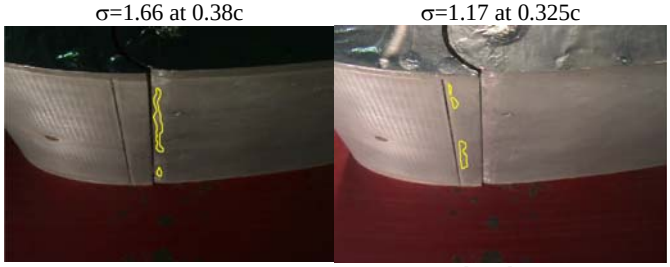

Open gap Closed gap

Deflection angle of 0^o

σ=1.48 at 0.38c σ=1.40 at 0.325c

Open gap Closed gap

Deflection angle of 3^o

σ=1.70 at 0.35c σ=1.43 at 0.305c

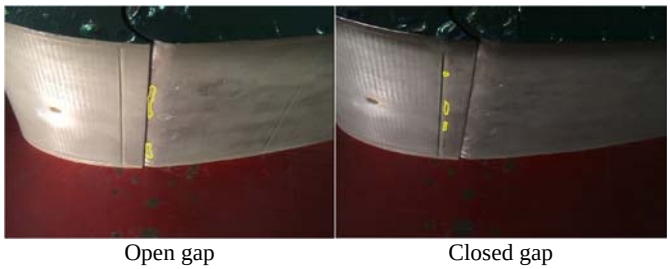

Open gap Closed gap

Deflection angle of 5^o

Figure 25: Cavitation inception of the horn section

Table 3 Comparison cavitation locations and incipient numbers of the pintle section between open and closed gap (c : chord)

Deflection angle	Open gap cavitation inception No. (location)	Closed gap cavitation inception No. (location)
0	1.02 (0.41c)	1.09 (0.41c)
3	1.74 (0.455c)	1.40 (0.41c)
5	1.46 (0.455c)	1.35 (0.41c)

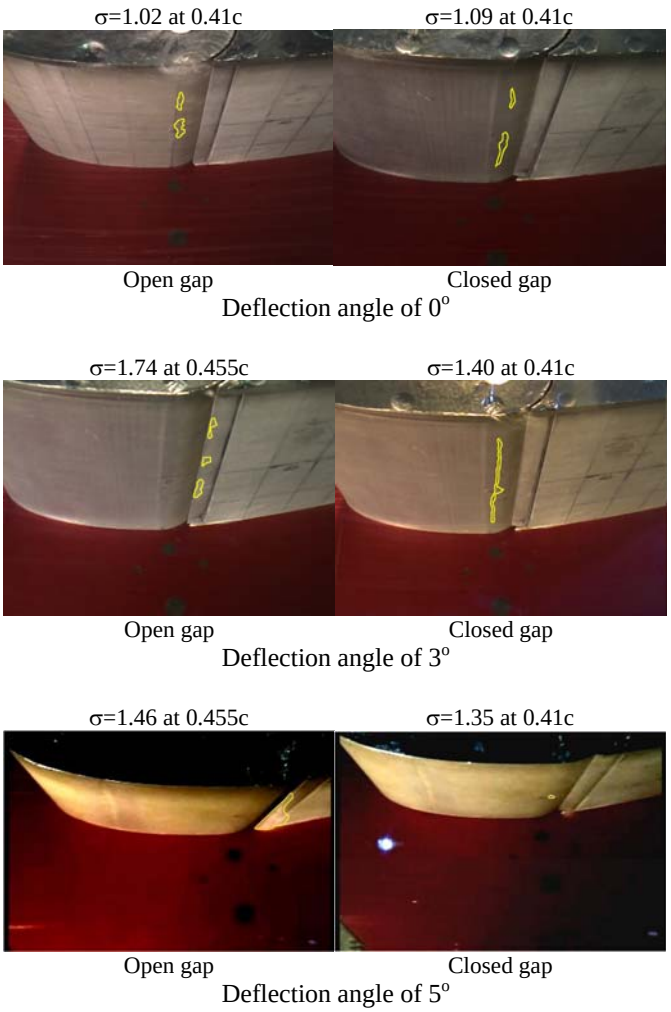

Figure 26: Cavitation inception of the pintle section

In the computational results for the surface pressure (Figure 13 ~ Figure 16), the possible incipient cavitation locations were well matched to those of the cavitation visualization tests (Table 4 and Table 5). However, while the incipient cavitation numbers in horn section were well match, those in pintle section wasn't. It is conjectured that grids near the gap of the sharp edge of the movable flaps in the pintle section is not enough.

Table 4: Comparison results of the incipient cavitation location and numbers between experiments and computations for the horn section

Deflection angle	Open gap cavitation inception No. (location)		Closed gap cavitation inception No. (location)	
	Exp.	CFD	Exp	CFD
0	1.66 (0.38c)	1.07 (0.366c)	1.17 (0.325c)	0.98 (0.32c)
3	1.48 (0.38c)	1.40 (0.366c)	1.40 (0.325c)	1.23 (0.32c)
5	1.70 (0.35c)	1.67 (0.365c)	1.43 (0.325c)	1.52 (0.32c)

Table 5: Comparison results of the incipient cavitation location and numbers between experiments and computations for the pintle section

Deflection angle	Open gap cavitation inception No. (location)		Closed gap cavitation inception No. (location)	
	Exp.	CFD	Exp	CFD
0	1.02 (0.41c)	0.84 (0.4c)	1.09 (0.41c)	0.83 (0.4c)
3	1.74 (0.455c)	1.08 (0.46c)	1.40 (0.41c)	1.15 (0.41c)
5	1.46 (0.455c)	1.24 (0.455c)	1.35 (0.41c)	1.35 (0.41c)

CONCLUSION

A new rudder system configuration was devised and proposed with cavitation suppression and lift augmentation in mind. Model tests were conducted to verify the design concept of the new devices. In the surface pressure measurements, it is found that the gap flow is blocked well by the gap flow control devices, so the pressure differences between suction and pressure side of each model was increased. In the cavitation visualization tests, it is confirmed that the gap flow control devices can suppress the cavitation near the gap of each model. In conclusion, experimental and computational results display the mechanism of the lift augmentation and cavitation suppression and warrant further study for inclusion of the interactions with hull and propellers, and mechanical design for manufacturing and operations.

ACKNOWLEDGEMENT

This work was supported by the Korea Research Foundation Grant (KRF - 2005 - 005 - J01603) and the Korea Science and Engineering Foundation (KOSEF) grant funded by the Korea government (No. ROA-2007-000-10028-0).

REFERENCES

[1] Kim, M.C., Lee, U.S., and Byun, T.Y. (2008). 'Study on Optimization of Anti-erosion Rudder Section of Large Container Ship by Genetic Algorithm'. Journal of the Society of Naval Architects of Korea **45**(3), pp.403-410. (In Korean)

[2] Shen, Y.T., Jiang, C.W., and Remmers, K.D. (1997). 'A Twisted Rudder for Reduced Cavitation'. J. Ship Research **41**(4), pp.260-272.

[3] Boo, G.T., Song, I.H., and Shin, S.C. (2003). 'Numerical Simulation for the Rudder in order to Control the Cavitation Phenomena'. Proceedings of International Workshop on Frontier Technology in Ship and Ocean Engineering, Seoul, Korea.

[4] Paik, B.G., Kim, K.Y., Ahn, J.W., Kim, Y.S., Kim, S.P., and Park, J.J. (2008). 'Experimental study on the gap entrance profile affecting rudder gap cavitation'. Ocean Engineering **35**, pp.139-149

[5] Choi, J-E, and Chung, S-H (2007). "Characteristics of Gap Flow of a 2-Dimensional Horn-type Rudder Section", J. of the Society of Naval Architects of Korea, Vol.44, No.2, pp.101-110 (In Korean).

[6] Park, S, Heo, J, and Yu, B (2007). "Numerical Study on Horn Rudder Section to Reduce Gap Cavitation," Proc. 10th Int. Sympo. on Practical Design of Ships and Other Floating Structures (PRADS2007), Vol.2, Houston, USA, pp. 1255-1260.

[7] Kim, S, Park, J, Kim, Y, Jang, Y, Choi, Y, and Paik, B (2006). "An Experimental Research on Gap Cavitation Erosion of Semi-spade Rudder," J. of the Society of Naval Architects of Korea, Vol.43, No.5, pp.578-585 (In Korean).

[8] Rhee, S.H., and Kim, H., 2008, *A suggestion of gap flow control devices for the suppression of rudder cavitation,* J. Marine Science and Technology, Vol. 13.

[9] Shih, T-H, Liou, WW, Shabbir, A, Yang, Z, and Zhu, Z (1995). "A New k-ε Eddy-Viscosity Model for High Reynolds Number Turbulent Flows - Model Development and Validation," Computers Fluids, Vol. 24, No. 3, pp. 227-238.

[10] Kim, S-E, and Rhee, SH (2002). "Assessment of Eight Turbulence Models for a Three-Dimensional Boundary Layer Involving Crossflow and Streamwise Vortices," AIAA Paper 2002-0852, Proc. 40th AIAA Aerospace Sciences Meeting and Exhibit, Reno, NV, USA.

[11] Rhee, SH, Makarov, B, Krishnan, H, and Ivanov, V (2005). "Assessment of Volume of Fluid Method for Free-Surface Wave Flows," J. of Marine Science and Technology, Vol. 10, No. 4, pp.173-180.